

Elsevier Editorial System(tm) for Biosensors  
and Bioelectronics  
Manuscript Draft

Manuscript Number:

Title: Nanodiamonds on tetrahedral amorphous carbon significantly enhance dopamine detection and cell viability

Article Type: SI:Biosensors 2016

Section/Category: The others

Keywords: Nanodiamonds; tetrahedral amorphous carbon; dopamine; biocompatibility

Corresponding Author: Dr. Emilia Peltola,

Corresponding Author's Institution: Aalto University

First Author: Emilia Peltola

Order of Authors: Emilia Peltola; Niklas Wester; Katherine B Holt; Leena-Sisko Johansson; Jari Koskinen; Vesa Myllymäki; Tomi Laurila

## Nanodiamonds on tetrahedral amorphous carbon significantly enhance dopamine detection and cell viability

Emilia Peltola <sup>a,b,\*</sup>, Niklas Wester <sup>c</sup>, Katherine B. Holt <sup>b</sup>, Leena-Sisko Johansson <sup>d</sup>, Jari Koskinen <sup>c</sup>, Vesa Myllymäki <sup>e</sup>, Tomi Laurila <sup>a</sup>

<sup>a</sup> Department of Electrical Engineering and Automation, School of Electrical Engineering, Aalto University, PO Box 13500, 00076 Aalto, Finland

<sup>b</sup> Department of Chemistry, University College London, Gordon Street 20, London WC1H 0AJ, UK

<sup>c</sup> Department of Materials Science and Engineering, School of Chemical Technology, Aalto University, PO Box 16200, 00076 Aalto, Finland

<sup>d</sup> Department of Forest Products Technology, School of Chemical Technology, Aalto University, PO Box 11000, 00076 Aalto, Finland

<sup>e</sup> Carbodeon Ltd. Oy, Pakkalankuja 5, 01510 Vantaa, Finland

\*) Corresponding author: emilia.peltola@aalto.fi, +358 50 435 4505

### Abstract

We hypothesize that by using integrated carbon nanostructures on tetrahedral amorphous carbon (ta-C), it is possible to take the performance and characteristics of these bioelectrodes to a completely new level. The integrated carbon electrodes were realized by combining nanodiamonds (NDs) with ta-C thin films. NDs were functionalized with mixture of carboxyl and amine groups ND<sub>andante</sub> or amine ND<sub>amine</sub>, carboxyl ND<sub>vox</sub> or hydroxyl groups ND<sub>H</sub> and drop-casted or spray-coated onto substrate. By utilizing these novel structures we show that (i) the detection limit for dopamine can be increased by two orders of magnitude [from 10  $\mu$ M to 50 nM] in comparison to ta-C thin film electrodes and (ii) the coating method significantly affects electrochemical properties of NDs and (iii) the ND coatings selectively promote cell viability. ND<sub>andante</sub> and ND<sub>H</sub> showed most promising electrochemical properties. The

viability of human mesenchymal stem cells and osteoblastic SaOS-2 cells was increased on all ND surfaces, whereas the viability of mouse neural stem cells and rat neuroblastic cells was improved on ND<sub>andante</sub> and ND<sub>H</sub> and reduced on ND<sub>amine</sub> and ND<sub>vox</sub>. The viability of C6 cells remained unchanged, indicating that these surfaces will not cause excess gliosis. In summary, we demonstrated here that by using functionalized NDs on ta-C thin films we can significantly improve sensitivity towards dopamine as well as selectively promote cell viability. Thus, these novel carbon nanostructures provide an interesting concept for development of various in vivo targeted sensor solutions.

**Keywords** Nanodiamonds; tetrahedral amorphous carbon; dopamine; biocompatibility

## 1. Introduction

A bulk diamond exhibits a unique combination of chemical, physicochemical and mechanical properties. Diamond-like carbon is a class of amorphous carbon material that displays some of the typical properties of diamond due to the significant amounts of sp<sup>3</sup> hybridized carbon atoms in the structure. In biological applications the benefits of diamond-like carbon include the stability, biocompatibility (Myllymaa et al. 2010, Kaivosoja et al. 2013a, Kaivosoja et al. 2013b) and the ability to resist bacterial adhesion (Myllymaa et al. 2013). Tetrahedral amorphous carbon (ta-C) is the form of diamond-like carbon, which is the hardest, strongest, and slickest. ta-C has a water window of 3.7 V; making it an attractive sensor material as a wide water window enables a large operational range for analyte detection in water based solutions (Kaivosoja et al. 2014). Moreover, we have recently demonstrated improved sensitivity towards dopamine (DA) with ta-C electrodes (Kaivosoja et al. 2013c, Laurila et al. 2014).

Unfortunately, ta-C per se is not sensitive enough for achieving clinically meaningful detection limits for typical target molecules, such as DA. However, it is possible to build on top of ta-C hybrid carbon nanostructures that exhibit very good selectivity and excellent sensitivity toward DA (Sainio et al. 2015a, Sainio et al. 2015b). We hypothesize that by using hybrid carbon structures, it is possible to take the performance and characteristics of the bioelectrodes to a completely new level as well as to enhance tissue response.

Here, we combine ta-C with nanodiamonds (ND). Detonation NDs ranging from 4 nm to 6 nm in size are produced by detonation of carbonaceous explosives (Schrand et al. 2009, Dolmatov 2001). NDs have a wide range of potential applications in tribology, drug delivery, bioimaging and tissue engineering, and also as protein mimics and a filler material for nanocomposites (reviewed in Krueger (2008), Mochalin et al. (2012)).

Low concentrations NDs are typically considered biocompatible (Schrand et al. 2007a, Huang et al. 2014), but unattached nanoparticles can have toxic effects to cells at high concentrations ( $>50 \mu\text{g/ml}$  (Solarska-Ściuk et al. 2014)  $>200 \mu\text{g/ml}$  (Thomas et al. 2012)), mainly due to their easy penetration into cells. The effect of interaction seems to depend on the type of nanoparticles, their size, concentration, and time of incubation and also on cell type. However, compared to other carbon nanostructures, such as carbon black and carbon nanotubes, the NDs possess a better biocompatibility when in contact with neuronal and lung cell lines (Schrand et al. 2007b). To the authors' knowledge, the biocompatibility of ND coatings has not been investigated extensively.

One of major issues limiting the function of the implantable sensor is biofouling and the formation of a scar-like capsule around sensors, which lead to reduced analyte diffusion and perfusion to implanted sensors which ultimately causes a decrease in sensor response (Wisniewski, Reichert 2000). Typically insufficient regeneration of the local tissue results in the formation of a fibrous or glial scar, which reducing the effective transfer of signal and compromises recording or stimulation. For a better performance of the biosensors, the material should promote regeneration of the target tissue and suppress fibrous or glial cell growth. Here we will investigate the effect of ND coatings on several different cell types.

From the electrochemical point of view, the behaviour of NDs is interesting. The core of each ND is crystalline diamond, with trace nitrogen incorporation from the precursor material, while the outer several layers consists both  $\text{sp}^3$  and  $\text{sp}^2$  bonded carbon atoms resulting in a more complex structure (Holt 2014).

NDs have been applied in electrochemistry by sintering ND powder (Novoselova et al. 2004), preparing electrodes by binding the ND powder with mineral oil and immobilising a thin layer onto a glassy carbon electrode (Holt et al. 2008), and drop casting from an ethanol solution (Holt et al. 2008, Holt 2010). Previous experiments with oxidized and hydrogenated NDs demonstrate that the oxidised particles (including the untreated particles) show increased redox activity in comparison to the

hydrogenated powder (Holt et al. 2008). The results suggest that the electrochemical response of the ND is dependent on the surface chemistry of the particles, with no contribution from the bulk.

Here, we investigate the different surface functionalities of NDs and their effect on electrochemical detection of DA as well as cell viability.

## 2. Materials and Methods

### 2.1. Sample fabrication

The ta-C sample were prepared on p-type conductive Si substrates (0.001–0.002  $\Omega\text{cm}$ , Ultrasil, USA), which were cleaned by standard RCA cleaning method followed by ultrasonication for 3 min in HPLC grade acetone (Sigma Aldrich). First, a 20 nm of Ti was deposited by direct current magnetron sputter (DC-MS) followed by 7 nm ta-C film deposited by pulsed filtered cathodic vacuum arc (p-FCVA) (described in Palomäki et al. (2015)). The following deposition parameters were used for Ti: discharge power fixed at 100 W, total pressure 0.67 Pa, Ar gas flow rate of 29 sccm, and deposition time of 350 s at a distance of 220 mm. For the ta-C film p-FCVA deposition system (Lawrence Berkeley National Laboratory, USA) equipped with a 45° bent magnetic filter to reduce macroparticle contamination and two cathodes in a dual cathode configuration was used. Graphite cathodes (Goodfellow) of 99.95% purity were used and a pulse forming network (PFN) was used to strike the triggerless arc (Anders et al. 1998) with a frequency of 1 Hz. The PFN was controlled with custom-made National Instruments hardware and LabView software. The 2.6 mF capacitor bank was charged to 400 V resulting in an arc current of 0.7 kA and 0.6 ms pulse width. The total pressure during the ta-C deposition process was below  $1 \times 10^{-4}$  Pa.

During the depositions the samples were at floating potential and rotation (20 rpm) was used to ensure homogeneous film deposition. The deposition rates for Ti and ta-C films were determined by contact profilometry (Dektac XT). After deposition wafers were diced into 1x1 cm chips with an automated dicing saw.

Four types of functionalized NDs: zeta-positive  $\text{ND}_{\text{andante}}$  with amino and carboxyl functional groups, zeta positive amino functionalized  $\text{ND}_{\text{amine}}$ , carboxyl functionalized zeta-negative  $\text{ND}_{\text{vox}}$  and zeta positive hydrogen terminated  $\text{ND}_{\text{H}}$  (Carbodeon uDiamond®, Carbodeon, Vantaa, Finland) were investigated. The NDs were coated on ta-C substrates using a spraying technique as well as drop

casting. The nanodiamond-water solutions with concentrations of 5 wt-% ( $ND_{\text{andante}}$ ,  $ND_{\text{vox}}$ ), 0.99 wt-% ( $ND_{\text{amine}}$ ) and 2.5 wt-% ( $ND_{\text{H}}$ ) were diluted in ethanol to prepare a solution with 0.05 wt-%. The spraying was done with pressurized air as carrying gas from a distance of 10 cm and the scanning was repeated ten times, the pressure being 3.5 bars. Drop cast samples were prepared by pipetting 40  $\mu\text{l}$  of 0.05 wt-% water solutions of the nanodiamonds on ta-C substrates placed on glass slides on a hotplate preheated to 85 °C and dried for 10 min.

## 2.2. Physical characterization of samples

Surface chemical composition was evaluated with X-ray photoelectron spectroscopy (XPS, AXIS Ultra electron spectrometer by Kratos Analytical, Manchester, UK), using monochromated Al  $K\alpha$  X-ray irradiation at 100 W under neutralisation. Wide energy survey spectra as well as high resolution regional spectra of carbon C 1s, oxygen O 1s and nitrogen N 1s were recorded after overnight pre-evacuation, together with ash-free cellulose filter paper as an *in-situ* reference (Johansson et al. 2005). Fitting of high resolution data was done using CasaXPS software, assuming Gaussian line shapes. The binding energies were charge corrected with the help of Zr 3d at 182.2 eV and the above mentioned cellulose reference (with the aliphatic component at 285.0 eV).

Raman spectroscopy was performed using LabRAM HR (Jobin Yvon Horiba) confocal Raman system. Argon laser ( $\lambda = 488$ , Power = 10 mW) with a BX 41 (Olympus) microscope and 100 x objective with spot size around 1  $\mu\text{m}$  was used for all samples. Collection aperture was set to 500  $\mu\text{m}$  to maximize the intensity of the diamond peak.

The sample morphology was studied with atomic force microscopy (AFM) using scanning probe microscopy (Ntegra Aura, NT-MDT Company, Russia). The measurements were carried out in contact mode with a PtIr-coated conductive probe (CSG30/Pt, NT-MDT Company, Russia).

## 2.2. Electrochemical measurements

Scanning electrochemical microscopy (SECM) measurements were carried out using CHI910B scanning electrochemical microscope (CH Instruments). 2  $\mu\text{m}$  and 10  $\mu\text{m}$  platinum wires sealed in glass were used as the working electrode, an Ag/AgCl electrode served as a reference electrode and a platinum wire as a counter electrode. Approach curves and SECM images were recorded using a steady

state voltage of 400 mV for the working electrode and 1 mM FcMeOH (Sigma) in 0.15 M H<sub>2</sub>SO<sub>4</sub> was used as a mediator. SECM experimentation consists of recording approach curves where the normalized current  $I = i/i_{\text{inf}}$  is plotted versus the normalized distance  $L = d/a$ , where  $i$  is the current at the tip electrode (radius  $a$ ) localized at a distance  $d$  from the substrate,  $i_{\text{inf}}$  is the steady-state current when the tip is at an infinite distance from the substrate. The approach rate was 2  $\mu\text{m s}^{-1}$ . The fittings between experimental and theoretical curves were done following C. Lefrou's approximations (Cornut, Lefrou 2008) based on Bard-Mirkin's formalism, where tips parameters ( $a$  and  $R/G$ ) were determined independently from approach curves of an insulator sample. A dimensionless rate constant  $\kappa = k_{\text{eff}}a/D$ , where  $k_{\text{eff}}$  is an apparent heterogeneous charge transfer constant between the mediator in solution and the substrate and  $D$  diffusion constant, was obtained from the theoretical approach curves. SECM imaging was recorded in feedback mode. Approach curves and imaging were repeated three times.

Before cyclic voltammetry with Gamry Reference 600 potentiostat, circular area was defined from the sample with a PTFE tape (Irpola Oy, Finland). A conventional three electrode cell with an Ag/AgCl (Radiometer Analytical) and a glassy carbon counter electrode was used. Electron transfer properties were probed with 1 mM FcMeOH in 0.15 M H<sub>2</sub>SO<sub>4</sub>. DA hydrochloride (Sigma-Aldrich) was dissolved in phosphate buffered saline (PBS, pH 7) and different volumes of 0.05, 0.05 and 10 M DA solutions were injected into 50 ml PBS solution. The injected volumes were kept in the  $\mu\text{L}$  range and increase in volume was compensated for. The electrodes were rinsed in PBS between each measurement and the solution was stirred by bubbling nitrogen after injection.

The solutions were deaerated with N<sub>2</sub> for at least 15 minutes before measurements and the cell was kept at N<sub>2</sub> overpressure during the measurements. All solutions were prepared on the day of the measurement.

### 2.3. Cell culture

For cell culture experiments, the samples were sterilized in 70% ethanol in Petri dishes for 10 min, after which most of the ethanol was removed, followed by evaporation for 20 min.

Cells were cultured in humidified incubator with 5% CO<sub>2</sub> in the air. Human mesenchymal stem cells (hMSC, Poietics<sup>TM</sup>, Lonza, Basel, Switzerland) were cultured in Lonza MSC-basal medium with mesenchymal cell growth supplement (MSCGM) containing L-glutamine, osteoblastic SaOS-2 (ECACC 890500205) cells in McCoy's 5A culture medium supplemented with 2 mM L-glutamine and

10% foetal bovine serum, mouse neural stem cells (mNSC, ATCC® CRL2926™) in Eagle's Minimum Essential Medium supplemented with 2 mM L-Glutamine and 10 % FBS). PC12 (adherent type, ATCC® CRL1721.1™) rat neuroblastic cells and C6 (ATCC® CCL-107™) rat glial cells were cultured in F12-K medium supplemented with 2.5% FBS and 15% horse serum. All media were supplemented with antibiotics, Gentamicin/Amphotericin-B for MSCGM and 100 IU/ml of penicillin and 100 µg/ml of streptomycin for all other media.

The seeding densities followed the recommended seeding densities for each cell type and were 5 000 cells cm<sup>-2</sup> for hMSCs, 20 000 cells cm<sup>-2</sup> for SaOS-2 cells, 30 000 cells cm<sup>-2</sup> for mNSC and PC12 cells and 70 000 cells cm<sup>-2</sup> for C6 cells. Cells were cultured for 24 h.

The viability rate of cells was tested by 3-(4,5-dimethylthiazol-2-yl)-2,5-diphenyltetrazolium bromide (MTT) assay. After culture, the samples were transferred to a clean 24-well plate and 1 mg/ml of MTT was added in the medium. After 3 h incubation at 37°C in a humidified chamber, the medium was removed and MTT was dissolved in 500 µl of isopropanol. 400 µl samples were transferred to a clean 24-well microplates and the absorbance was read with an automated plate reader at 570 nm (FLUOstar Optima, Ortenberg, Germany). Data was collected from triplicate samples.

The cell morphology was evaluated with actin and nuclei visualization. Samples were washed twice in PBS and fixed in 4% paraformaldehyde (PFA) in PBS for 10 min, followed by washing in PBS, permeabilization in for 10 min in 0.1% Triton X-100 in PBS, and washing in the same solution. Non-specific binding sites were blocked 0.1% bovine serum albumin in PBS for 1 hour. Samples were incubated for 1 h in Phalloidin-586 (Biotium), washed in PBS and mounted in Vectashield mounting medium with DAPI (Vector laboratories). Cells were observed with Olympus BX51M microscope equipped with Leica DFC420 camera.

### **3. Results and Discussion**

The elemental composition of the drop-casted NDs is presented in Table 1 and the high resolution C 1s spectra in Figure 1. Carbon lines were surprisingly broad, suggesting chemical shifts or charging problems. However, elemental contents of nitrogen and oxygen were particularly low (~2%) on ND<sub>amine</sub> and ND<sub>H</sub>, confirming that the C 1s broadening was not due to chemical shift. Moreover, the shifts were not originating from charging, as this would have affected all the features in XPS spectra while in this case both Zr 3d and N 1s signals remained sharp and uncharged. So we propose that this



broadening was due to electrochemical properties of the samples. In this case, peak fitting would not be unambiguous. However, oxygen functionalities in ND<sub>vox</sub> (which has 3-4 times more oxygen than the other ND types) show up in C 1s peak which is clearly shifted towards higher binding energies.

Furthermore, the ND<sub>andante</sub> had ca. 50% more oxygen than ND<sub>amine</sub> and ND<sub>H</sub>, confirming the presence of oxygen. The presence of amino groups in ND<sub>amine</sub> could not be reliably verified by XPS as there were no significant differences in nitrogen content or N 1s peak shape between the ND types. For comparison, amino functionalization of ta-C resulted in approximately 50% increase in the amount of nitrogen observed in XPS spectrum (Kaivosoja et al. 2015). It is probable that the heat treatment used during drop casting causes partial denaturation of the ND functionalization. The differences observed in electrochemical properties between drop casted and spray coated samples, as discussed later, support this conclusion.

The Raman spectrum (Figure 1) suggests the presence of sp<sup>2</sup> rich amorphous carbon. The spectrum represents that of ta-C with Raman D and G bands centering at 1554 cm<sup>-1</sup> and 1400 cm<sup>-1</sup> (Laurila et al. 2015), with the addition of first-order diamond Raman peak at 1332 cm<sup>-1</sup> originating from the ND cores.

AFM image (Figure 1) confirmed the even distribution of the spray-coated NDs on the surface whereas the drop casting method resulted in distinct coffee ring effect (not shown). The thickness of the spray-coated ND layer was estimated from cross-sectional SEM images to be approximately 100 nm.

### 3.1. Electrochemistry

The approach curves exhibit positive feedback in FcMeOH (Figure 2) on all surfaces. This is slightly surprising considering the insulating nature of the diamond core of NDs. However, the more complex outer layer structure, which consists of both sp<sup>2</sup> and sp<sup>3</sup> hybridized carbon, explains the conductivity of the ND coating. Furthermore, the ta-C surface is always sp<sup>2</sup> rich despite the amount of sp<sup>3</sup> in the underlying bulk, thus resulting into reasonable high surface density of states (DOS) (Sainio et al. 2016). This together with the small thickness of the ta-C film (7 nm) ensure that the electron transfer and transport through the film are feasible.

The apparent charge transfer rates  $\kappa$  derived from the SECM approach curves demonstrate increased charge transfer for ND<sub>andante</sub> ( $\kappa=1.8\pm0.1$ ) and ND<sub>H</sub> ( $\kappa=1.9\pm0.2$ ) and decreased charge transfer for ND<sub>amine</sub> ( $\kappa=1.4\pm0.1$ ) and ND<sub>vox</sub> ( $\kappa=1.3\pm0.1$ ) compared to the uncoated ta-C reference sample

( $\kappa=1.48\pm 0.02$ ). The ta-C sample demonstrate less variance than those for the ND samples due to the homogeneous and smooth nature of ta-C. Cyclic voltammogram confirms the difference of electron transfer kinetics of the various ND functionalities.  $\text{ND}_{\text{andante}}$  and  $\text{ND}_{\text{hydrogen}}$  show almost reversible electrode kinetics ( $\Delta E_p$  64 mV and 62 mV, respectively), whereas  $\text{ND}_{\text{amine}}$  ( $\Delta E_p$  404 mV) and  $\text{ND}_{\text{vox}}$  ( $\Delta E_p$  303 mV) showed irreversible and quasireversible electrode kinetics, respectively (Figure 2, Table 1).

The FcMeOH redox reactions should not be largely affected by surface functionalities as FcMeOH is an outer-sphere redox probe. Therefore, the difference must origin from the structure of the ND coatings. The functionalization may alter the structure of the outer carbon layers, e.g.  $sp^2$  and  $sp^3$  hybridization, and affect the surface density of states. On the other hand, the difference may be explainable by minor changes in packaging of the coating. For example, the surface structure may create steric hindrance so that the analyte cannot approach the surface of  $\text{ND}_{\text{amine}}$  and  $\text{ND}_{\text{vox}}$  as affectively as  $\text{ND}_{\text{andante}}$  or  $\text{ND}_{\text{H}}$ . Moreover, previous research has reported that increase in the charge transfer rates of in ND nanoparticle surface (drop-casted) compared to ND film (chemical vapor deposition) can be due to the higher relative concentrations of electrode transfer sites due to the higher surface to bulk atom ratio of the nanoparticles (Holt et al. 2009). The  $\text{ND}_{\text{H}}$  can be expected to be slightly smaller in size than the other NDs whereas  $\text{ND}_{\text{andante}}$  has functionalities capable of interacting (easily resulting in agglomeration). Therefore, these two possibly form denser structure than  $\text{ND}_{\text{amine}}$  and  $\text{ND}_{\text{vox}}$ .

The SECM images (Figure 3) demonstrate the highly heterogeneous surface of all ND coatings. Notably, the approach curves were recorded with a 10  $\mu\text{m}$  tip averaging the area represented in Figure, which was recorded with a 2  $\mu\text{m}$  tip. Comparing the SECM images to the topography recorded by AFM (Figure 1), it seems possible that the electrochemical properties follow the topographical features of the sample to a certain degree. However,  $\text{ND}_{\text{andante}}$  and  $\text{ND}_{\text{H}}$  represent current range from negative ( $i/i_{\text{inf}} < 1$ ) to positive ( $i/i_{\text{inf}} > 1$ ) feedback, indicating true heterogeneity of the surfaces.

Interestingly, in earlier research, oxygenated NDs were found to exhibit the greatest electrochemical activity, followed by undoped ND, whereas the hydrogenated ND showed the lowest electrochemical activity towards  $\text{Fe}(\text{CN})_6^{4-/3-}$  and  $\text{Ru}(\text{NH}_3)_6^{3+/2+}$  (Holt et al. 2008). For  $\text{Fe}(\text{CN})_6^{4-/3-}$  this could be expected as it is surface sensitive redox couple (McCreery 2008).  $\text{Ru}(\text{NH}_3)_6^{3+/2+}$ , instead is an outer sphere redox couple and therefore this result seems to contradict our finding. Here the poor

performance of ND<sub>vox</sub> is possibly affected by the substrate. Both ta-C and ND<sub>vox</sub> are negatively charged (zeta potential for ta-C is -70 mV (Kaivosoja et al. 2013b) and -45 mV for ND<sub>vox</sub> at pH 7) which causes electrical repulsion. Indeed, we observed that both drop-casted and spray-coated ND<sub>vox</sub> detached from the surfaces during cycling. Moreover, spray-coated ND<sub>amine</sub> demonstrated changes in electrochemical behaviour over time. The zeta positive ND<sub>amine</sub> should interact strongly with the ta-C surface and therefore it is not obvious what happens to the coating during cycling. That this did not happen for drop-casted ND<sub>amine</sub> indicates the denaturation of the nitrogen surface functionalities during drop-casting. This may affect the observed electrochemical behaviour to some extent.

The detection of DA was investigated both on drop-casted and spray-coated ND surfaces. The drop-casted NDs showed increased sensitivity towards DA (Figure 4, Table 1). The detection limit for DA was decreased by two orders of magnitude (from 10  $\mu$ M (Kaivosoja et al. 2014) to 50 nM) in comparison to ta-C thin film electrodes. ND<sub>H</sub> showed the lowest detection limit (50 nM) for DA, followed by ND<sub>andante</sub> and ND<sub>amine</sub> (100 nM). The DA detection limit for ND<sub>vox</sub> was an order of magnitude higher (500 nM) than for ND<sub>H</sub>. Overall, the drop-casted ND electrodes did not produce clear peaks at low concentrations and show relatively slow electron transfer kinetics ( $\Delta E_p > 190$  mV for 100  $\mu$ M DA and  $\Delta E_p > 260$  mV for 1 mM DA).

Interestingly, the spray-coated NDs demonstrate significantly different behaviour from drop-casted NDs (Figure 4). The spray-coated ND<sub>andante</sub> and ND<sub>H</sub> resembled their drop-casted pairs, but the oxidation peak is shifted to higher anodic potential and the slope is less steep, both indicating slower reaction kinetics. Moreover, the reduction peak of the spray-coated samples is larger as the chemical reaction of dopamine quinone cyclization to leucodopaminechrome has less time to occur allowing dopamine quinone reduction back to dopamine. Furthermore, the background current is increased (3  $\mu$ A vs 2  $\mu$ A). Consequently, the sensitivity of spray-coated samples is decreased (1  $\mu$ M for ND<sub>andante</sub> and ND<sub>H</sub>) compared to their drop-casted pairs. The effect of the coating method on electrochemical properties was more evident with ND<sub>amine</sub> and ND<sub>vox</sub>, as the spray-coated samples did not produce oxidation or reduction peaks even at high concentrations of DA. We further tested the hypothesis that the difference may be partially due to the denaturation of functional groups during the heat treatment used in drop-casting by using cathodic pre-treatment of ND<sub>amine</sub> to reduce the amount of nitrogen. Previous research has shown that cathodic pre-treatment resulted in a reduction in the amount of nitrogen in amorphous carbon nitride films (Benchikh et al. 2012). After cathodic reduction (1V, 1 min), spray-coated ND<sub>amine</sub> demonstrated oxidation and reduction peaks for DA similar to those

observed on drop-casted ND<sub>amine</sub> (not shown). This supports the claim that ND<sub>amino</sub> functionalities were denaturated during drop casting. Other types of NDs might not be as significantly affected by the heat treatment but it is likely that some denaturation occurred at least also on ND<sub>vox</sub>.

In conclusion, the deposition method can significantly affect the electrochemical properties of functionalized NDs. Moreover, the packaging of NDs on the surface may be as important for the electrochemical behavior as are surface functionalities.

### 3.2. Cell viability

The spray-coated ND coatings influenced significantly the viability of different cell types (Figure 5). Actin cytoskeleton (fluorescence microscopy) appeared normal on all surfaces (not shown). The ND coatings improved the viability of MSCs by 53% and SaOS-2 cells by 31% with no statistically significant differences observed among the various NDs. mNSC and PC12 cells showed the largest variation in their viability, viability increasing over 50% on ND<sub>H</sub> surface and over 20% on ND<sub>andante</sub> surface and decreasing on ND<sub>vox</sub> and ND<sub>amine</sub> surfaces, down to 90% for mNSCs and to 50% for PC12 compared to ta-C reference. The viability of C6 cells remained unchanged, indicating that ND surfaces will not cause excess gliosis.

For hMSCs and SaOS-2 cells the increased viability might be simply due to the increased surface roughness since no differences were observed between different ND groups. The ta-C surfaces are smooth with an average roughness of 1.15 nm (Tujunen et al. 2015), whereas the ND surfaces are significantly rougher. Osteoblastic cells are generally known to prefer rough surfaces over smooth ones (Anselme 2000). C6 did not respond to surface roughness as the viability of C6 was similar on ta-C and ND surfaces. This is consistent with previous literature, as it has been reported that different roughness scales did not affect cellular proliferation of glial cells (Pennisi et al. 2009).

The difference in mNSC and PC12 viability is more likely to be explained by the effect of surface functionalities than surface roughness. ND<sub>vox</sub> and ND<sub>amine</sub> consist of homogeneous functionalities which may have resulted over dominance of some proteins on the surface and lack of some others. This is explained by the Vroman effect, which postulates that small and abundant molecules will be the first to coat a surface, but will be replaced over time by molecules with higher affinity for that particular surface (Vroman, Adams 1969a, Vroman, Adams 1969b). ND<sub>andante</sub> provides both carboxyl and amino functionalizes resulting in more heterogeneous surface than the homogeneous ND<sub>amine</sub> or ND<sub>vox</sub>,

whereas ND<sub>H</sub> does not offer specific binding sites for proteins. Therefore, it is possible that ND<sub>amine</sub> and ND<sub>vox</sub> surfaces present over dominance of some proteins and lack of others resulting in decreased cell viability.

In conclusion, the ND<sub>andante</sub> and ND<sub>H</sub> showed most promising electrochemical properties and these two surfaces could also be useful for supporting neural differentiation over glial differentiation. This could potentially result in improved tissue integration and prevent the glial scar formation therefore guaranteeing an effective transfer of signal and stability of implant. Moreover, patterning surfaces with NDs could also be used as an additional guide for cell growth. The NDs coated with drop-casting method resulted in strong coffee-ring effect, which clearly guided the cell growth (results not shown). Although ND<sub>amine</sub> or ND<sub>vox</sub> did not show a promising effect on the cells, the functional groups could be exploited for immobilization of proteins that would support the target tissue regeneration and guide cell differentiation into desired lineage. Moreover, the functionalized NDs can be utilized as an immobilization platform for biomolecules that are needed for the detection of electrochemically inactive species, such as glucose oxidase for glucose detection.

#### **4. Conclusions**

In summary, we demonstrated here that by using functionalized NDs on ta-C thin films we can significantly improve sensitivity towards DA and selectively promote cell viability. We also demonstrated that deposition method can significantly affect the electrochemical behavior of ND coatings. Hence, these novel hybrid carbon nanostructures provide an interesting concept for development of various in vivo targeted sensor solutions.

#### **Acknowledgements**

Academy of Finland (E.P. grant #274670, T.L. grants #285015 and #285526 and J.K. grant #259595), and Orion Research Foundation (E.P.) are acknowledged for funding. Dr. Vera Propotova is acknowledged for AFM imaging and M.Sc. Sami Sainio for ND coatings and cross-sectional SEM imaging.

#### **References**

- Anders, A., Brown, I.G., MacGill, R.A., Dickinson, M.R., 1998. *J. Phys. D* 31, 584–587.
- Anselme, K., 2000. *Biomaterials* 21, 667–681.
- Benchikh, A., Debiemme-Chouvy, C., Cachet, H., Pailleret, A., Saidani, B., Beaunier, L., Berger, M.H., Deslouis, C., 2012. *Electrochim. Acta* 75, 131–138.
- Cornut, R., Lefrou, C., 2008. *J. Electroanal. Chem.* 621, 178–184.
- Dolmatov, V.Y., 2001. *Russ. Chem. Rev.* 70, 607–626.
- Holt, K.B., 2014. Electrochemistry of nanodiamond particles, in: Williams, O.A. (Ed.), *Nanodiamond*. Royal Society of Chemistry, Cambridge, pp. 128–150.
- Holt, K.B., 2010. *Phys. Chem. Chem. Phys.* 12, 2048–2058.
- Holt, K.B., Ziegler, C., Caruana, D.J., Zang, J., Millán-Barrios, E.J., Hu, J., Foord, J.S., 2008. *Phys. Chem. Chem. Phys.* 10, 303–310.
- Holt, K.B., Ziegler, C., Zang, J., Hu, J., Foord, J.S., 2009. *J Phys. Chem. C* 113, 2761–2770.
- Huang, Y., Kao, C., Liu, K., Huang, H., Chiang, M., Soo, C., Chang, H., Chiu, T., Chao, J., Hwang, E., 2014. *Sci. Rep.* 4, 6919.
- Johansson, L., Campbell, J.M., Fardim, P., Hultén, A.H., Boisvert, J., Ernstsson, M., 2005. *Surf. Sci.* 584, 126–132.
- Kaivosoja, E., Berg, E., Rautiainen, A., Palomäki, T., Koskinen, J., Paulasto-Kröckel, M., Laurila, T., 2013c. *Conf Proc IEEE Eng Med Biol Soc.* 2013, 632–634.
- Kaivosoja, E., Myllymaa, S., Takakubo, Y., Korhonen, H., Myllymaa, K., Konttinen, Y.T., Lappalainen, R., Takagi, M., 2013b. *J Biomater. Appl.* 27, 862–871.
- Kaivosoja, E., Sainio, S., Lyytinen, J., Palomäki, T., Laurila, T., Kim, S.I., Han, J.G., Koskinen, J., 2014. *Surf. Coat. Tech.* 259, 33–38.
- Kaivosoja, E., Suvanto, P., Barreto, G., Aura, S., Soininen, A., Franssila, S., Konttinen, Y.T., 2013a. *J Biomed. Mater. Res. A* 101, 842–852.
- Kaivosoja, E., Tujunen, N., Jokinen, V., Protopopova, V., Heinilehto, S., Koskinen, J., Laurila, T., 2015. *Talanta* 141, 175–181.

- Krueger, A., 2008. *Chem. Eur. J.* 14, 1382–1390.
- Laurila, T., Rautiainen, A., Sintonen, S., Jiang, H., Kaivosoja, E., Koskinen, J., 2014. *Mater. Sci. Eng. C* 34, 446–454.
- Laurila, T., Sainio, S., Jiang, H., Palomäki, T., Pitkänen, O., Kordas, K., Koskinen, J., 2015. *Diamond Relat. Mater.* 56, 54–59.
- McCreery, R.L., 2008. *Chem. Rev.* 108, 2646–2687.
- Mochalin, V.N., Shenderova, O., Ho, D., Gogotsi, Y., 2012. *Nature Nanotech.* 7, 11–23.
- Myllymaa, K., Levon, J., Tiainen, V., Myllymaa, S., Soininen, A., Korhonen, H., Kaivosoja, E., Lappalainen, R., Konttinen, Y.T., 2013. *Coll. Surf B*, 101, 290–297.
- Myllymaa, S., Kaivosoja, E., Myllymaa, K., Sillat, T., Korhonen, H., Lappalainen, R., Konttinen, Y.T., 2010. *J Mater. Sci. Mater. Med.* 21, 329–341.
- Novoselova, I.A., Fedoryshena, E.N., Panov, ÉV., Bochechka, A.A., Romanko, L.A., 2004. *Phys. Solid State* 46, 748–750.
- Palomäki, T., Chumillas, S., Sainio, S., Protopopova, V., Kauppila, M., Koskinen, J., Climent, V., Feliu, J.M., Laurila, T., 2015. *Diamond Relat. Mater.* 59, 30–39.
- Pennisi, C.P., Sevcencu, C., Dolatshahi-Pirouz, A., Foss, M., Hansen, J.L., Larsen, A.N., Zachar, V., Besenbacher, F., Yoshida, K., 2009. *Nanotechnology* 20, 385103.
- Sainio, S., Nordlund, D., Caro, M.A., Gandhiraman, R., Koehne, J., Wester, N., Koskinen, J., Meyyappan, M., Laurila, T., 2016. *J. Phys. Chem. C* 120, 8298–8304.
- Sainio, S., Palomäki, T., Rhode, S., Kauppila, M., Pitkänen, O., Selkälä, T., Toth, G., Moram, M., Kordas, K., Koskinen, J., Laurila, T., 2015a. *Sens. Act. B* 211, 177–186.
- Sainio, S., Palomäki, T., Tujunen, N., Protopopova, V., Koehne, J., Kordas, K., Koskinen, J., Meyyappan, M., Laurila, T., 2015b. *Mol. Neurobiol.* 52, 859–866.
- Schrand, A.M., Dai, L., Schlager, J.J., Hussain, S.M., Osawa, E., 2007b. *Diamond Relat. Mater.* 16, 2118–2123.
- Schrand, A.M., Hens, S.A.C., Shenderova, O.A., 2009. *Crit. Rev. Solid State Mater. Sci.* 34, 18–74.

- Schrand, A.M., Huang, H., Carlson, C., Schlager, J.J., Osawa, E., Hussain, S.M., Dai, L., 2007a. *J. Phys. Chem. B* 111, 2–7.
- Solarska-Ściuk, K., Gajewska, A., Glińska, S., Michlewska, S., Balcerzak, Ł, Jamrozik, A., Skolimowski, J., Burda, K., Bartosz, G., 2014. *Chem. Biol. Interact.* 222, 135–147.
- Thomas, V., Halloran, B.A., Ambalavanan, N., Catledge, S.A., Vohra, Y.K., 2012. *Acta Biomater.* 8, 1939–1947.
- Tujunen, N., Kaivosoja, E., Protopopova, V., Valle-Delgado, J.J., Österberg, M., Koskinen, J., Laurila, T., 2015. *Mater. Sci. Eng. C* 55, 70–78.
- Vroman, L., Adams, A.L., 1969a. *Surf. Sci.* 16, 438–446.
- Vroman, L., Adams, A.L., 1969b. *J. Biomed. Mater. Res.* 3, 43–67.
- Wisniewski, N., Reichert, M., 2000. *Coll. Surf. B* 18, 197–219.



## Figure legend

Figure 1: Characterization of nanodiamonds. A) High resolution XPS C 1s spectrum of drop-casted nanodiamonds. The grey vertical line marks the position of aliphatic C-C. B) Raman spectrum of the spray-coated nanodiamonds. The vertical lines indicates the first-order diamond Raman peak at  $1332\text{ cm}^{-1}$ . C) AFM image of spray-coated ta-C ND<sub>andante</sub>.

Figure 2: FcMeOH electrochemistry on nanodiamonds. The approach curves recorded in 1 mM FcMeOH with 10  $\mu\text{m}$  Pt tip on (A) ND<sub>andante</sub>, (B) ND<sub>amine</sub>, (C) ND<sub>vox</sub>, (D) ND<sub>H</sub> and (E) the reference ta-C. (F) Cyclic voltammetry of 1mM FcMeOH on different spray-coated ND functionalities.

Figure 3: Scanning electrochemical microscopy images recorded in feedback mode on nanodiamond surfaces using 2  $\mu\text{m}$  Pt electrode.

Figure 4: Dopamine detection using nanodiamonds. Left column shows the dopamine detection on drop-casted nanodiamonds and right column on spray-coated nanodiamonds. Cycling speed 50 mV/s.

Figure 5: Viability of cells on nanodiamonds. Viability of osteoblastic SaOS-2, human mesenchymal stem cells, mouse neural stem cells, neuroblastic PC12 cells and glial C6 cells on different nanodiamond surfaces compared to viability on uncoated ta-C surface.

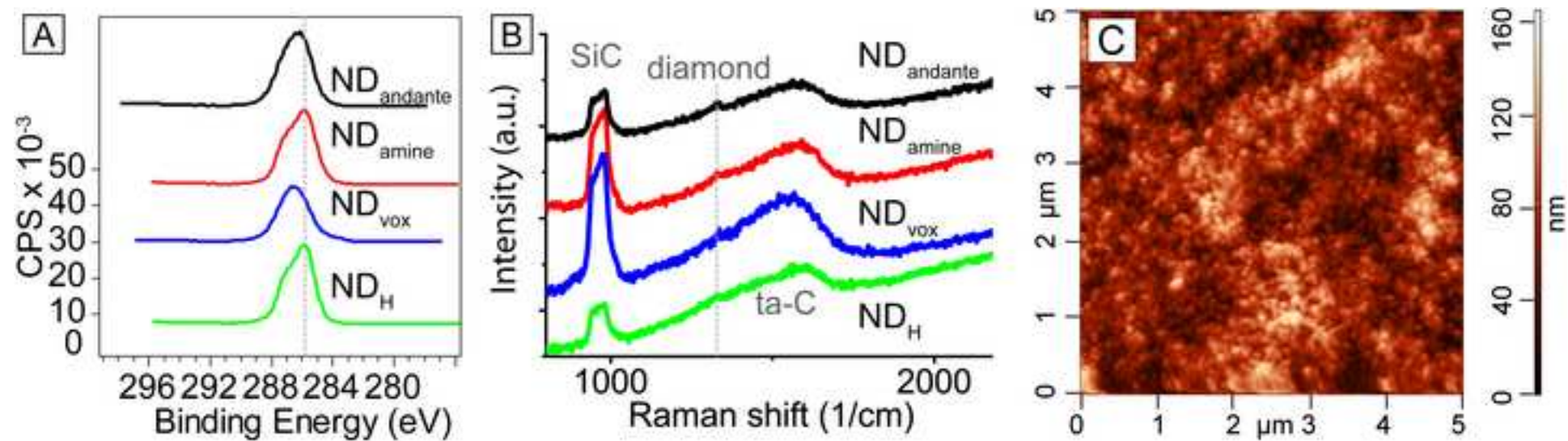
## Highlights

- By using ND coatings the detection limit for dopamine can be increased by two orders of magnitude [from 10  $\mu\text{M}$  to 50 nM] in comparison to ta-C thin film electrodes.
- Coating method significantly affects electrochemical properties of NDs.
- ND coatings selectively promote cell viability.

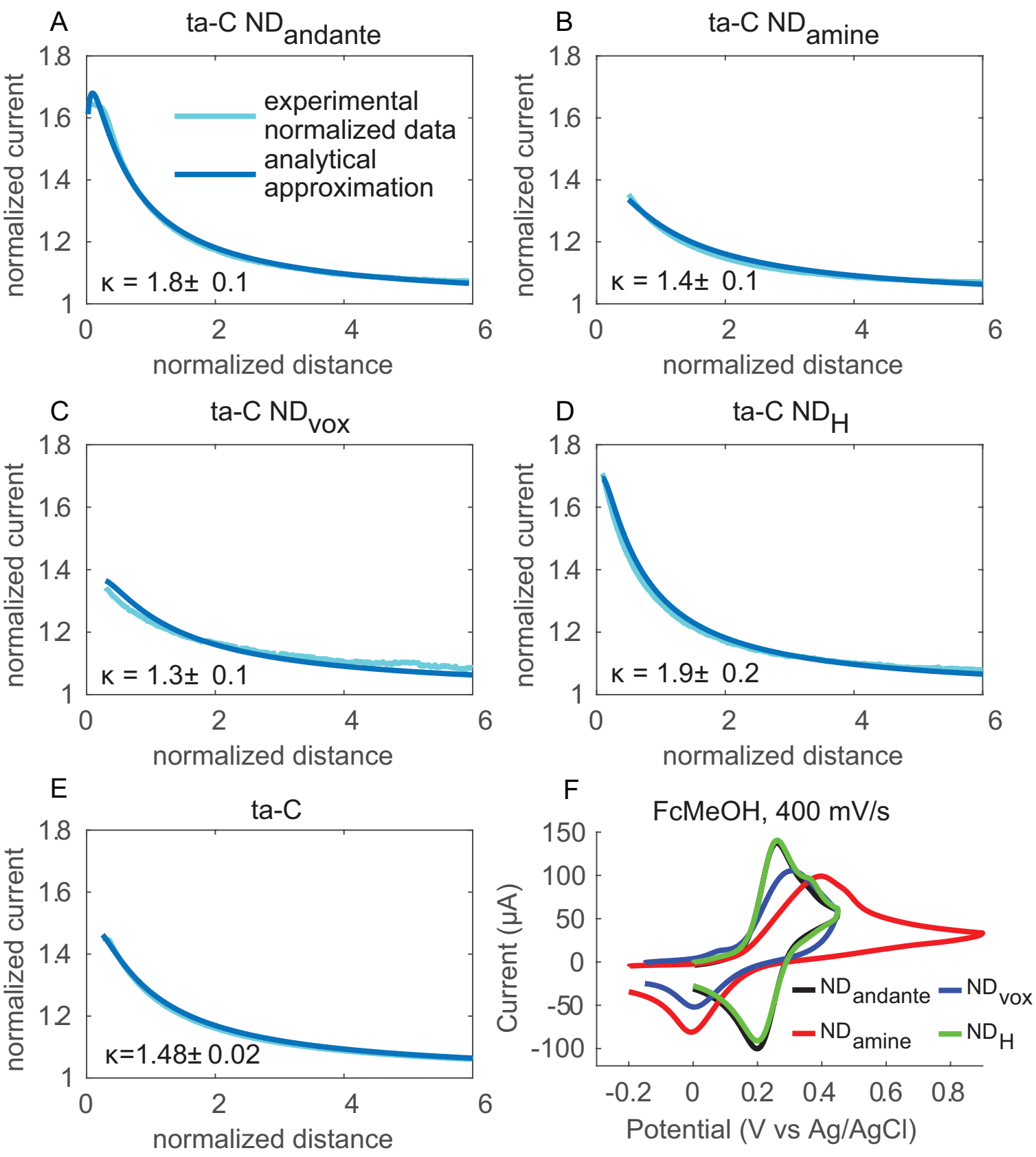
Table 1: XPS results of drop-casted nanodiamonds, electrochemical characterization of spray-coated nanodiamonds in FcMeOH and drop-casted nanodiamonds in dopamine.

<b>Electrode</b>	<b>C 1s</b>	<b>O 1s</b>	<b>N 1s</b>	<b>FcMeOH 400 mV/s <math>\Delta E_p</math> (1 mM)</b>	<b>DA <math>\Delta E_p</math> (100 <math>\mu</math>M)</b>	<b>DA <math>\Delta E_p</math> (1 mM)</b>	<b>DA detection limit</b>
ta-C + ND <sub>andante</sub>	94.5%	3.0%	1.4%	64 mV	198 mV	302 mV	100 nM
ta-C + ND <sub>amine</sub>	95.2%	1.8%	1.5%	404 mV	196 mV	260 mV	100 nM
ta-C + ND <sub>vox</sub>	88.0%	9.5%	1.8%	303 mV	310 mV	514 mV	500 nM
ta-C + ND <sub>H</sub>	95.4%	2.1%	1.5%	62 mV	192 mV	262 mV	50 nM

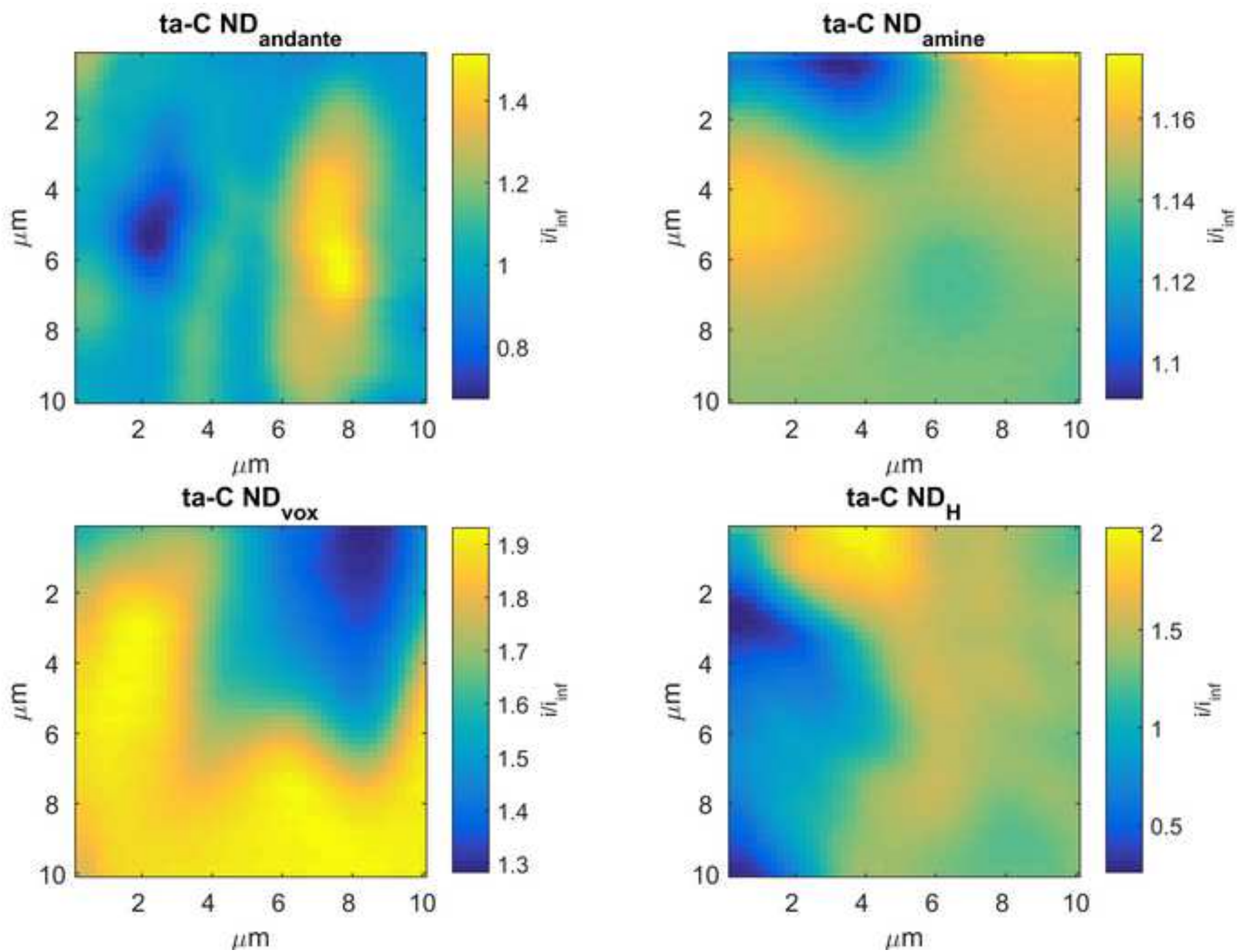
Figure(1)  
[Click here to download high resolution image](#)



Figure(2)



Figure(3)  
[Click here to download high resolution image](#)





Figure(5)

